Stepwise Decrease of Fluorescence *versus* Sequential Photobleaching in a Single Multichromophoric System

Abey Issac,[†] Richard Hildner,[†] Catharina Hippius,[‡] Frank Würthner,[‡,*] and Jürgen Köhler[†,*]

[†]Experimental Physics IV and Bayreuth Institute for Macromolecular Research (BIMF), University of Bayreuth, 95440 Bayreuth, Germany, and [‡]Institut für Organische Chemie and Center for Nanosystems Chemistry, Universität Würzburg, Am Hubland, 97074 Würzburg, Germany

ABSTRACT For individual molecules from the newly synthesized calix[4]arene tethered perylene bisimide (PBI) trimer, we studied the emitted fluorescence intensity as a function of time. Owing to the zigzag arrangement of PBI dyes in these trimers, the polarization state of the emission provides directly information about the emitting subunit within the trimer. Interestingly, we observed emission from *all* neutral subunits within a trimer rather than exclusively from the subunit with the lowest site energy. This can be understood in terms of thermally activated uphill energy transfer that repopulates the higher energetic chromophores. Together with the simultaneously recorded polarization-resolved emission spectra, this reveals that the emission from a multichromophoric system is governed by a complex interplay between the temporal variations of the photophysical parameters of the subunits, bidirectional hopping processes within the trimer, and unavoidable photobleaching. Moreover, it is demonstrated that the typically observed stepwise decrease of the signal from a multichromophoric system does not necessarily reflect sequential bleaching of the individual chromophores within the macromolecule.

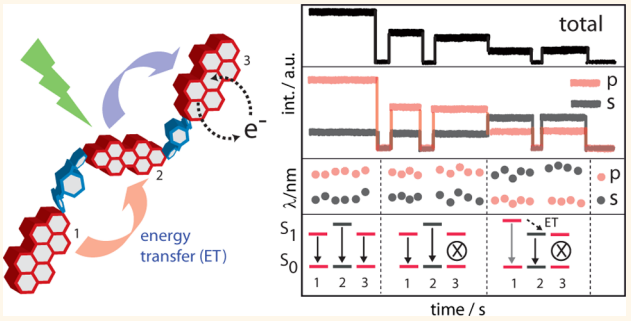

KEYWORDS: single-molecule spectroscopy · multichromophore · polarization-resolved emission spectra · excitation energy transfer · photobleaching · uphill energy transport

Exploitation of the features of organic matter for technological applications has become one of the greatest challenges in chemical physics during the last years.[1−16] In this regard multichromophoric systems play a prominent role, because their electronically excited states show interesting solid state effects such as migration of excitons or the formation of charge-transfer states that are directly related to fundamental as well as technologically challenging aspects of organic matter.[17−22] Hence, information about the fundamental photophysical properties of the molecular building blocks and their structure−property relationships are key for a detailed understanding of how fundamental electronic processes occur in nanoscale materials. However, large multichromophoric systems with great potential for applications appear very heterogeneous. Therefore, many research activities have been focused on small model systems with linear,[23,24] cofacial,[25] zigzag,[26,27] cyclic,[28] or square[29] geometries as well as dendrimers[30,31] consisting of 2 or more subunits. In particular, exploiting single-molecule spectroscopy techniques has been proven to be of great value for elucidating detailed information about the intramolecular energy transfer pathways in such systems.[23,32−44] From such studies, the picture emerged that the excitation energy in multichromophoric systems is transferred toward the chromophore with the lowest site energy from which the emission occurs.[32,39,40,42,44] As a consequence of this, the stepwise decrease of the fluorescence intensity as a function of time is commonly interpreted as a sequential photobleaching of the subunits within the multichromophore. Similarly, the spectral shift of the emission that often accompanies such an intensity step is associated as bleaching of the subunit with the lowest site energy.[32,45] Accordingly, this chromophore

* Address correspondence to juergen.koehler@uni-bayreuth.de, wuerthner@chemie.uni-wuerzburg.de.

Received for review November 26, 2013 and accepted January 20, 2014.

Published online January 20, 2014
10.1021/nn4060946

was populated most by energy transfer and therefore bleached first.

However, these interpretations need a critical assessment and generalizations should only be made with great care. For example, for some systems it has been reported that the number of photobleaching steps in an intensity trajectory differs from the number of subunits in a multichromophore.[23,27,44] Similarly, spectral shifts might not necessarily be a consequence of a preceding photobleaching event but could also be induced by conformational changes in the local environment.[43,46,47] And finally, at room temperature thermal energy is sufficient to induce back transfer to higher energy sites giving rise to a complex, bidirectional transport dynamics within a multichromophoric system rather than to a unidirectional energy transfer toward the subunit with the lowest site energy.

In this contribution, we present a single-molecule study on a newly synthesized small multichromophoric system consisting of three perylene bisimide (PBI) molecules that are covalently linked by calix[4]arene bridges, see Figure 1. From these trimers, we monitored simultaneously the emitted intensity and the emission spectra as a function of both time and polarization state. The intensity trajectories of single trimers show blinking, *i.e.*, a random succession of bright (emitting) and dark (nonemitting) periods, similar to other single quantum emitters in a disordered medium.[48−51] For organic molecules, photoinduced reversible formation of radical species is considered to be the origin of long-lived dark periods that cover a multitude of time scales (μs to s).[52−54] Given the large angle of 120° between the transition-dipole moments of the PBI subunits, polarization-resolved spectral measurements allow us to associate changes in the transition energies directly with the PBI subunits and to correlate intensity changes with the radical ion formation and/or photobleaching of a specific PBI building block.

Using three illustrative examples, we will demonstrate that conclusions about sequential photobleaching of individual subunits, which are based solely on the number of steps in the total intensity trajectory, are not reliable. We will present examples for both a stepwise decrease of the total intensity that is not at all related to stepwise photobleaching of the subunits, and *vice versa* a stepwise photobleaching that is not reflected in the total intensity trajectory. We rather find that the profile of an intensity trajectory is determined by a complex interplay between photobleaching, fluctuations of absorption cross sections and/or fluorescence quantum yields of the individual subunits, as well as temporal variations of energy transfer pathways and rates within the trimers. In particular, the competition between downhill energy transfer and thermally activated uphill energy transfer between the subunits cannot be neglected. Hence, prior to photobleaching of one of the PBI units, emission can occur from all photoactive PBI subunits within the trimer and not exclusively from the subunit with the lowest site energy.

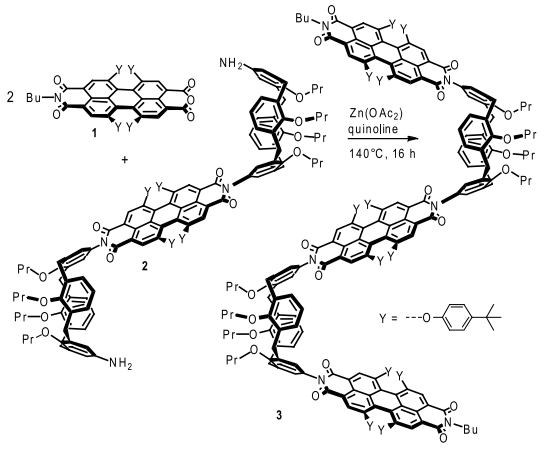

Figure 1. Synthesis of the perylene bisimide (PBI) trimer (3). Three PBI chromophores are covalently linked through a tetrakis(propyloxy)-calix[4]arene. The angle between the $S_1 \leftrightarrow S_0$ transition-dipole moments of adjacent PBI chromophores is about 120° and the center-to-center distance between the chromophores is about 22 Å.

RESULTS

Synthesis. PBI trimer **3** was prepared according to our previous synthetic protocol for the synthesis of oligomeric PBI-calix[4]arene arrays,[25,26] Figure 1. Accordingly, the freshly prepared diamino-calix[4]arene PBI **2** was reacted with 5 equiv of perylene imide anhydride **1** in quinoline in the presence of zinc acetate to give PBI trimer **3** in an isolated yield of 31% after standard column chromatography and successive preparative high performance liquid chromatography (HPLC). The compound was fully characterized by proton NMR spectrometry and MALDI-TOF as well as high resolution ESI-TOF mass spectrometry (see synthesis of PBI **3** and Figure S1 in the Supporting Information). The purity was confirmed by analytical HPLC and UV/vis spectroscopy, where the PBI trimer showed an extinction coefficient that perfectly matches the 3-fold value of the calix[4]arene-connected PBI monomer, Figure S2.

Ensemble Experiments. The peak-normalized absorption and emission spectra of PBI-monomer and trimer molecules dissolved in toluene are displayed in Figure 2. The absorption spectra feature a maximum at 573 nm and a shoulder at 533 nm corresponding to the purely electronic $S_1 \leftarrow S_0$ (0−0) transition and the transitions into the vibrational levels of S_1 (0−1), respectively. The absorption band at shorter wavelengths (400−475 nm) is associated with the transition into a higher excited singlet state ($S_2 \leftarrow S_0$). The emission spectra of PBI-monomers and trimers show a main band centered at 602 nm and a shoulder around 640 nm that correspond to the purely electronic transition $S_1 \rightarrow S_0$ (0−0), and the transitions into

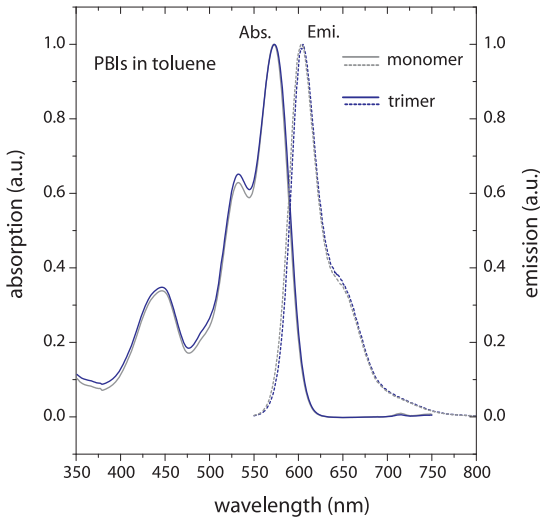

Figure 2. Absorption (full line) and emission (dashed line) spectra of PBI trimers (blue) and monomers (gray). All spectra have been normalized to their peak.

the vibrational levels of the electronic ground state ($S_1 \rightarrow S_0$, 0−1), respectively. The small spectral red-shift of 3 nm (*ca.* 80 cm^{-1}) from the monomer to the trimer emission is probably caused by the additional calix-[4]arene-bridge within the trimers that slightly changes the dielectric properties in the local surrounding of the PBI subunits with respect to the monomers. Nevertheless, the almost similar absorption and emission spectra of PBI-monomer and trimer molecules indicate a weak electronic interaction between the PBI subunits within the trimers, both in the ground state and in the electronically excited states. The notion of weak coupling in the trimers is in agreement with our finding for the corresponding PBI-dimer system, where we estimated $V/\Delta \ll 1$ for the ratio of the electronic interaction strength V and the energetic mismatch Δ between the site energies of the subunits.[41,43] Since the trimer comprises the same PBI units and calix[4]arene-bridges as the dimer system, and because the geometry between neighboring PBIs is very similar in dimers and trimers, it is plausible to consider also the trimers as a weakly coupled system, in which the excitation energy is localized on individual PBI subunits.

Single-Molecule Experiments. As a first example for a trajectory of an individual trimer, we show in Figure 3a the total intensity, *i.e.*, $I = (I_p + I_s)$, for a trimer with *three* different signal levels labeled *i* (0−49.8 s), *ii* (52.5−137.7 s), and *iii* (138−164.7 s). From the polarization-resolved intensity trajectories I_p and I_s (Figure 3b, red and gray lines), it is obvious that during the time interval *i* and *ii* the I_p channel shows two distinct signal levels, whereas the signal in the I_s channel remains almost constant. During the time interval *iii*, the signals in the I_p and I_s channels change in an anticorrelated way: a decrease of I_p is accompanied by an increase of I_s and *vice versa*. The

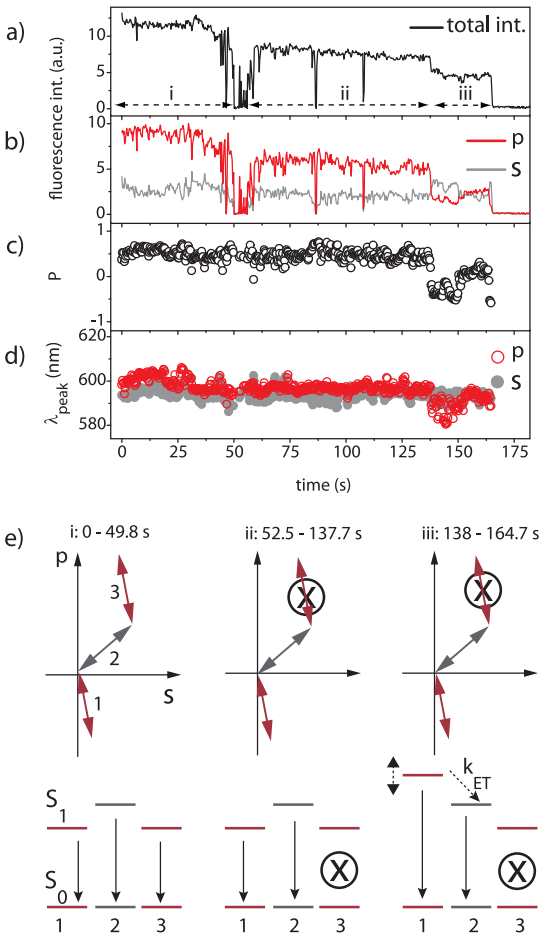

Figure 3. (a) Total intensity trajectory ($I_p + I_s$). The three signal levels *i*, *ii*, and *iii* are marked with horizontal double-headed arrows. (b) Intensity trajectory of I_p (red) and I_s (gray). (c) Polarization ratio *P* calculated from the data shown in (b). (d) Spectral peaks (λ_{peak}) of the polarization-resolved emission spectra (p, red open circle; s, gray filled circle). (e) From left to right: three situations that correspond to the three time intervals *i*−*iii*. Top: Projections of the transition-dipole moments of the three PBI subunits, 1 (dark red), 2 (dark gray), and 3 (dark red), of a trimer into the focal plane. Bottom: Relative positions of the energies of the first excited singlet states for the three PBI subunits. The crossed circles refer to a permanently photobleached PBI subunit. In the rightmost panel, the vertical double headed arrow indicates temporal variations of the energy of the S_1 state of PBI subunit 1, and k_{ET} suggests excitation energy transfer between the neutral PBI subunits 1 and 2. See text for details.

corresponding polarization ratio, $P = (I_p - I_s)/(I_p + I_s)$, is depicted in Figure 3c. The means (standard deviation, SD) of *P* for the time periods *i*, *ii*, and *iii* are 0.51 (0.11), 0.46 (0.12), and −0.14 (0.25), respectively. Note that *P* varies between positive and negative values in the time period *iii*, which reflects the anticorrelated intensity change in the mutually orthogonal polarized intensity channels. The peak emission wavelengths, λ_{peak}, of the polarization-resolved emission spectra are shown in Figure 3d as a function of time (see Figure S3 in the Supporting Information for typical polarization resolved spectra). During periods *i* and *ii*, λ_{peak} is rather

constant in both channels, with the signal in the s-channel being slightly blue-shifted relative to that in the p-channel. During period *iii*, λ_{peak} of the s-channel is still rather constant, whereas that of the p-channel exhibits first a blue-shift followed by a red-shift. For the p-channel, the means (SD) of λ_{peak} amount to 599 nm (3.3 nm), 597 nm (1.5 nm), and 590 nm (3.9 nm) for the intervals *i*, *ii*, and *iii*, respectively. Similarly, for the s-channel, the means (SD) of λ_{peak} are 594 nm (2.4 nm), 594 nm (2.2 nm), and 593 nm (1.8 nm) for these intervals.

Looking only at the total intensity as a function of time, Figure 3a, an obvious interpretation for the observed three intensity steps would be a sequential bleaching of the individual PBI-subunits in this single trimer. However, this interpretation is not in line with the additional information from the polarization-resolved trajectories and spectra. For example, during period *iii*, the polarization ratio *P* changes as a function of time which is not in agreement with the interpretation that the lowest signal level originates from a single emitter. In this case, the change in *P* could only occur if the whole trimer is rotating, which is highly unlikely for such a large system in a rather rigid polymer matrix (we verified that the polarization ratio of an individual PBI-monomer does not change as a function of time, see Figure S5c,g). Moreover, during the first half of period *iii*, different λ_{peak} values are observed for the emission spectra in the p- and s-channels, which is a clear indication for the presence of more than one emitter during this time window.

In the following we will present a model that describes consistently the above-mentioned observations. The $S_1 \leftrightarrow S_0$ transition-dipole moments are oriented along the long axes of the PBI-subunits, and thus lie in a plane (see the molecular structure in Figure 1). Because the molecules are detected optically by their emission signal, we preferentially observe trimers that are predominantly oriented in a plane perpendicular to the optical axis. Then, the mutual orientations of the projections of the PBI transition-dipole moments onto this plane, as depicted in Figure 3e, correspond basically to the molecular structure shown in Figure 1. In this situation, the acquisition of polarization-resolved spectra allows us to identify directly the relative orientations of the transition-dipole moments as well as the relative site energies of the emitting subunits from the differences in the peak emission wavelengths.

During the time interval *i* (0−49.8 s), the intensity in the p-channel is nearly a factor of 2 higher than that in the s-channel, Figure 3b. This suggests that initially all the three subunits are in the emissive state and that subunits 1 and 3 (with mutually parallel transition-dipole moments) are oriented nearly parallel to the p-axis of the laboratory frame, Figure 3e top left. Moreover, as the λ_{peak} values are different for p- and s-polarizations with a slightly blue-shifted emission of the s-channel with respect to that in the p-channel, Figure 3d, we can infer that the $S_1 \rightarrow S_0$ transition energy is highest for subunit 2 and about equal for subunits 1 and 3, Figure 3e bottom left. During the next interval *ii* (52.5−137.7 s), only the intensity of the p-channel is reduced, while still observing different λ_{peak} values in both channels, Figure 3d. This hints for the bleaching of one of the outer PBI subunits, say 3. This situation is depicted in Figure 3e center, where the crossed circle refers to the bleached PBI subunit. Also during interval *iii* (138−164.7 s), where the total emission intensity is reduced to about 1/3 of its initial level, we observe different λ_{peak} values in the two polarization channels, which provides clear evidence for two independently emitting subunits, here denoted as 1 and 2. Hence, this second step cannot arise from a second bleaching event, but might rather reflect modifications in the absorption cross sections and/or emission quantum yields of the remaining neutral subunits. This interpretation is supported by the emission spectra that show strongly fluctuating λ_{peak} values, particularly in the p-channel, during period *iii*. Because this channel is associated with the outer subunit 1 that is more exposed to the polystyrene host than the central one, the observed changes of the absorption/emission properties are likely matrix induced,[43,46,47] see also the Discussion section below. Another interesting aspect in period *iii* is the correlation between site energy (*i.e.*, λ_{peak}) variations and changes in the polarization resolved intensity trajectories. In the first half of period *iii*, the blue-shifted emission in the p-channel with respect to the emission in the s-channel (Figure 3d) testifies that the $S_1 \rightarrow S_0$ transition energy of subunit 1 exceeds that of subunit 2, see Figure 3e bottom right. At the same time, the fluorescence intensity is higher in the s-channel, Figure 3b, which is mainly associated with the emission from subunit 2. During the second half of period *iii*, this difference in transition energies disappears, because both λ_{peak} values are about similar, and the intensity in the p-channel, which is mainly associated with emission from subunit 1, is now slightly higher. This correlation points toward a modification of the energy transfer efficiency between subunits 1 and 2 caused by changes of the site energy of subunit 1.

In the second example, we present a trimer that features only *two* distinct signal levels prior to permanent photobleaching, Figure 4a. However, because the polarization-resolved intensity trajectories reveal clearly three distinguishable segments for I_p and I_s, we divide the trajectory again into three periods *i* (0−30 s), *ii* (63.6−90.6 s), and *iii* (98.1−147 s), Figure 4b. For the time intervals *i* and *ii* the signal in the I_p channel is higher than that in the I_s channel. Further, in period *ii* the intensities of both polarization-resolved trajectories are reduced with respect to those observed during period *i*. During period *iii*, I_p is further

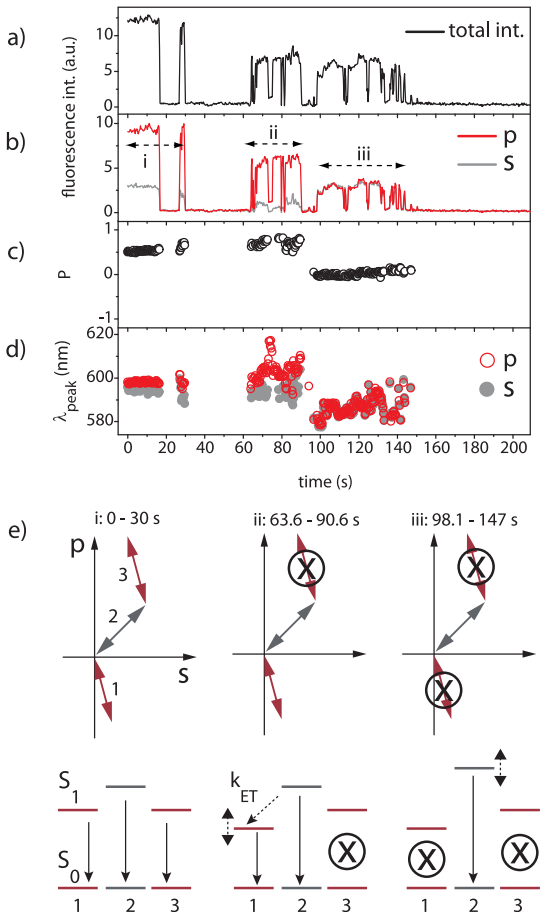

Figure 4. (a) Total intensity trajectory ($I_p + I_s$) of a single PBI trimer molecule that shows two different signal levels. (b) Intensity trajectory of I_p (red) and I_s (gray). Accordingly, the trajectories are divided into three intervals *i*, *ii*, *iii* marked with the horizontal double-headed arrows. (c) Polarization ratio *P* calculated from the data shown in (b). (d) Spectral peaks (λ_{peak}) of the polarization-resolved emission spectra (p, red open circle; s, gray filled circle). (e) From left to right: three situations that correspond to the three time intervals *i*–*iii*. The setup and the notations are similar to Figure 3.

reduced while I_s increases, resulting in signals of equal strength in both channels. Remarkably, now the intensity fluctuations of I_p and I_s are strongly correlated. The time dependence of the corresponding polarization ratio *P* is presented in Figure 4c and features means (SD) of 0.54 (0.05), 0.69 (0.07), and 0.01 (0.05) during the time intervals *i*, *ii*, and *iii*, respectively. For λ_{peak}, we find that in period *i* the emission in the p-channel is slightly red-shifted with respect to the s-channel, Figure 4d. During the next period *ii*, the emission in the p-channel (still red-shifted with respect to the s-channel) exhibits large spectral fluctuations of up to 25 nm. Finally, within time interval *iii*, the λ_{peak} values for both polarizations are blue-shifted with respect to the previous intervals and become identical. The λ_{peak} entries for the p-channel are characterized (means (SD)) by, 598 nm (0.90 nm), 603 nm (4.8 nm), and 586 nm (4.2 nm) for the periods *i*, *ii*, and *iii*, respectively. Similarly, the means (SD) of λ_{peak} for the s-channel amount to 594 nm (1.9 nm), 594 nm (3.2 nm), and 586 nm (4.2 nm) for these intervals.

These observations are consistent with the model that is schematically depicted in Figure 4e. The setup of the figure is similar to that of Figure 3e. Different intensity levels (Figure 4b) and distinct λ_{peak} values (Figure 4d) for the p- and s-polarization channels during interval *i* (0–30 s) suggest that initially all three PBI-subunits are photoactive, Figure 4e left. The rather large, stepwise decrease of the intensity in the p-channel between periods *i* and *ii* indicates that one of the outer subunits, *e.g.*, 3, is bleached as depicted in Figure 4e, center, with a crossed circle. The presence of two remaining, optically active subunits, *i.e.*, 1 and 2, is consistent with the observation of different λ_{peak} values in the two polarization channels during period *ii*. Moreover, during this interval, the $S_1 \rightarrow S_0$ transition energy of the outer subunit, *i.e.*, 1, is further lowered, as evidenced by the increased red-shift of λ_{peak} in the p-channel with respect to period *i*, Figure 4d. This favors efficient excitation energy transfer from the higher-energy subunit 2 to the lower-energy subunit 1, which results in the reduction of the fluorescence signal from subunit 2 during period *ii*, Figure 4b. During period *iii*, the observation of both the strongly correlated intensity fluctuations for I_p and I_s, as well as identical λ_{peak} values in the two polarization channels, Figure 4b,d, suggests that a second bleaching event occurred, and that now the detected emission stems solely from PBI-subunit 2. Interestingly, the intensity in the s-channel increases despite this bleaching event, Figure 4b. We attribute this observation to the termination of the energy transfer from subunit 2 to the previously neutral subunit 1. As a result, the fluorescence from subunit 2 is no longer quenched (Figure 4b) and the signal in the s-channel recovers to the level observed initially in period *i*.

Finally, we introduce a third example of a trimer molecule which shows just *one* signal level in the total intensity trajectory, Figure 5a. The polarization-resolved trajectories for I_p and I_s are presented in Figure 5b, and unlike the two previous examples, here the signal in the s-channel is strongest during the first 62.1 s. During the following period (62.4–179.1 s), the reverse is observed and the intensity fluctuations in both polarization channels are synchronized. Accordingly, we divide the trajectory into the time intervals *i* (0–62.1 s) and *ii* (62.4–179.1 s). The polarization ratio can be characterized (mean (SD)) by −0.45 (0.14) and 0.27 (0.08) during these intervals, Figure 5c. The peak emission wavelengths show generally strong spectral diffusion throughout the entire observation time. During period *i*, λ_{peak} is clearly different in both channels, with a red-shifted emission in the s-channel as compared to the p-channel. Toward the end of this interval, the λ_{peak}-values become similar, and in period *ii*, these

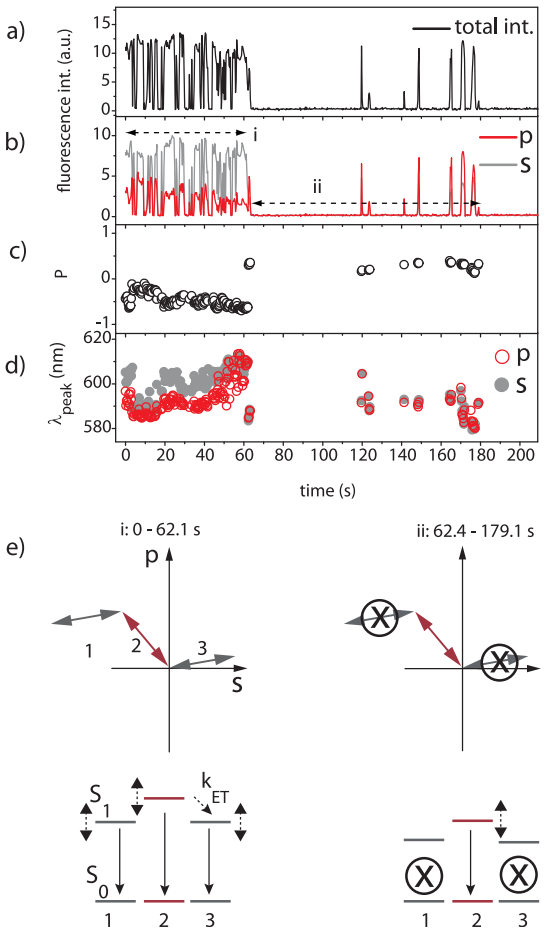

Figure 5. (a) Total intensity trajectory ($I_p + I_s$) of a single PBI trimer molecule that shows one signal levels. (b) Intensity trajectory of I_p (red) and I_s (gray). Accordingly, the trajectories are divided into two intervals *i* and *ii* marked with the horizontal double-headed arrows. (c) Polarization ratio *P* calculated from the data shown in (b). (d) Spectral peaks (λ_{peak}) of the polarization-resolved emission spectra (p, red open circle; s, gray filled circle). (e) From left to right: two situations that correspond to the two time intervals *i* to *ii*. The setup and the notations are similar to Figure 3.

are identical in both channels. The mean (SD) of λ_{peak}-values are 594 nm (7.3 nm), during period *i*, and 589 nm (5.7 nm), during period *ii*, for the p-channel, and 601 nm (7.0 nm), during period *i*, and 589 nm (5.7 nm), during period *ii*, for the s-channel, Figure 5d.

These observations can be understood as follows, Figure 5e. The high intensity observed for the s-channel, see Figure 5b, suggests that the outer subunits 1 and 3 are now inclined more toward the s-axis of the laboratory frame, in contrast to the previous examples. Given the different intensity levels as well as the different λ_{peak} values for the signals in the p- and the s-channels during interval *i* (0–62.1 s), it is plausible that initially all three PBI subunits emit independently, Figure 5e left. Because the emission in the p-channel is blue-shifted with respect to the emission in the s-channel, we conclude that the $S_1 \rightarrow S_0$ transition energy for subunit 2 is the highest allowing for energy transfer from subunit 2 to subunits 1 and/or 3. At the end of this period, *i.e.*, between 60.6 and 62.1 s, the λ_{peak} values for both polarizations shift to the red by up to 7 nm and become nearly identical. Similarly as discussed for the other two examples (Figures 3 and 4), these site energy variations induce a change of the energy transfer efficiency between the subunits that give rise to an increase of the p-channel emission at the expense of that in the s-channel, Figure 5b.

During the second interval (62.4–179.1 s), we observe correlated fluctuations for the intensities I_p and I_s, Figure 5b, and identical peak emission wavelengths for both polarizations. Therefore, we conclude that a collective bleaching event occurred and now the emission stems from a single subunit only. The higher intensity of the p-channel suggests that the subunits 1 and 3, *i.e.*, those that are more inclined toward the s-axis, have bleached, Figure 5e right. The higher intensity in the p-channel during this period (Figure 5b) can be attributed to two factors. First, the strong blue-shift of the emission of about 27 nm is likely to be accompanied by a similar blue-shift of the absorption spectrum of subunit 2. This would result in a larger absorbance at 532 nm and is in line with the increase of I_p. Second, termination of the energy transfer process from subunit 2 to subunits 1 and/or 3 due to the collective photobleaching event at the end of period *i* increases the fluorescence quantum yield of subunit 2 and hence I_p, consistent with previous reports that the formation of a photoproduct does not quench the fluorescence from the neutral subunits.[32,33,45]

In total, we investigated 95 individual trimers and 45% featured three signal levels, 25% showed two signal levels, and for 10% we observed a single signal level in the total intensity trajectories. Interestingly, for 20% of the cases, we found more than three signal levels, see Figure S6 and accompanying text for an example. Despite the more complex stepwise behavior of the total intensity trajectory, this case can be understood in complete analogy to the three examples discussed in Figures 3–5 above, *i.e.*, by an interplay between modifications of the absorption cross sections and/or of the fluorescence quantum yields of the subunits, as well as changes of the excitation energy transfer pathways and rates between neutral subunits that are induced by variations of their site energies.

DISCUSSION

In the weak coupling limit excitation-energy transfer occurs *via* incoherent hopping processes, and the transfer rate can be estimated using Fermi's Golden Rule (Förster approach). This approach yields an energy transfer rate between adjacent subunits in the trimer system of $k_{ET} \sim 7 \times 10^{10}\ s^{-1}$ (14 ps)$^{-1}$ based on an interaction strength of 40 cm^{-1},[41,43] and a spectral overlap between the absorption and emission calculated from the bulk spectra, Figure 2. This number is in good agreement with the nearest-neighbor transfer

rates measured for similar weakly coupled multichromophoric systems.[23,27,31,45] Since this value is 2 orders of magnitude faster than the radiative decay rate of PBI, which amounts to $(5.8\ \text{ns})^{-1}$, the emission from a single trimer is expected to originate from the PBI subunit with the lowest site energy irrespective of which subunit was excited. Such single-site emission has been demonstrated for various weakly coupled multichromophoric systems by observing photon-antibunching.[23,37,40,45,55] Hence, on first sight it appears straightforward to associate the multiple steps in the intensity trajectories of a multichromophoric system with a sequential bleaching of the optically active subunits. However, an important finding from our polarization-resolved emission spectra of single PBI-trimers is that the number of steps observed in the total intensity trajectories does not necessarily correspond to the number of emitting subunits and/or photobleaching events. For example, although the total intensity trajectory shown in Figure 3a exhibits three signal levels, the second stepwise intensity drop observed between time intervals *ii* and *iii* is not due to a second photobleaching event, but reflects a change in the absorption cross section and/or emission quantum yield of the subunits. Instead, sequential photobleaching of three PBI subunits can result in a two-step total intensity trajectory, see Figure 4a. For this particular trajectory, the total intensity during periods *ii* and *iii* is nearly constant, and a second photobleaching event is hardly seen. This would lead to the erroneous interpretations that either only two emitting subunits are present at the beginning of the observation time giving rise to a dimer-like intensity trajectory, or alternatively, that collective photobleaching of two subunits occurs at the end of period *i* resulting in a monomer-like blinking trajectory during periods *ii* and *iii*. In contrast, the polarization-resolved data clearly reveal a sequential three-step photobleaching of this trimer despite the two-step total intensity trajectory. Finally, a further level of complexity in the interpretation of the total intensity trajectories arises, because a collective photobleaching process of two subunits may not even result in a stepwise total intensity change, as demonstrated in the third example, Figure 5. This particular trajectory resembles that of a monomer, and might be misinterpreted as if only a single subunit of this trimer is optically active. Nevertheless, the polarization-resolved spectra and trajectories provide clear evidence for a collective photobleaching event taking place at the end of period *i*.

Another important observation in this work is that we detect emissions from *all* neutral subunits within the bin time of our experiment (300 ms), rather than *always* from the lowest energy site only. Given the fast energy transfer rate of about $(14\ \text{ps})^{-1}$ as estimated above, one would expect rapid population of the lowest energy site and subsequent emission exclusively from this subunit. Although simultaneous emission from all neutral subunits of a multichromophoric system was previously observed, this was attributed to an exceptional situation of excitation energy hopping among near-resonant subunits.[23,42,56] In our case, however, simultaneous emission from all subunits occurs even if the differences in site energies are large (up to $570\ \text{cm}^{-1}$). To understand this discrepancy, we have to consider two competing effects, *i.e.*, rapid energy transfer to lower energy sites and thermally activated repopulation of higher energy sites. From the differences (SD-values) of the peak emission wavelength provided in the three examples above, we can deduce a variation of the site energies between neutral PBI subunits between 140 and $570\ \text{cm}^{-1}$. An order of magnitude estimate yields that a difference in site energies of $570\ \text{cm}^{-1}$ increases the energy transfer rate to $(5\ \text{ps})^{-1}$ due to the improved spectral overlap between a higher-energy donor and a lower-energy acceptor site. Consequently, an increase in the site energy difference should be accompanied by a higher emission intensity from the PBI subunit with lower site energy (acceptor) at the expense of the intensity from the higher-energy site (donor). Indeed, such correlations between the variations in the $S_1 \rightarrow S_0$ transition energies and the changes in the intensities of the PBI subunits have been observed in all trajectories shown in Figures 3–5 (see also the Discussion below).

In contrast to this downhill energy transfer process, the thermal energy at room temperature, which amounts to $210\ \text{cm}^{-1}$, gives rise to an activated energy transfer in the opposite direction. Assuming detailed balance, the uphill energy transfer rate k_u is given by the (downhill) rate k_{ET} multiplied with the Boltzmann-factor:

$$k_u = k_{ET} \cdot e^{-\Delta E/k_B T} \quad (1)$$

where ΔE is the site energy mismatch between donor and acceptor subunits and $k_B T$ is the thermal energy. For typical site energy differences between 140 and $570\ \text{cm}^{-1}$, it follows that the uphill rates are only about a factor of 2–15 smaller with respect to the corresponding downhill rates. Consequently, the subunits with higher site energies will still be repopulated many times during the excited state lifetime of about 6 ns, *i.e.*, there is a finite probability that the emission occurs as well from higher-energy sites.

To illustrate these competing processes, we reconsider the example shown in Figure 3 during periods *ii* and *iii*, where only subunits 1 and 2, *i.e.*, a single donor–acceptor pair, are optically active (see also Figure S7 for a kinetic scheme of the energy transfer processes). During period *ii*, the λ_{peak} values indicate a mismatch in site energies of about $230\ \text{cm}^{-1}$. Here subunit 2 is the high-energy site and subunit 1 is the low-energy site (Figure S7a). For this situation,

we expect downhill energy transfer from subunit 2 to 1. This is consistent with the higher signal in the p-channel, Figure 3b, which is associated mainly with the emission from subunit 1. However, the finite emission from subunit 2 observed during the experimental bin time of 300 ms illustrates the thermal repopulation of this subunit within the excited state lifetime. This reasoning is corroborated by calculating the uphill energy transfer rate for an energy mismatch of 230 cm^{-1} which yields a value that is only a factor of 3 smaller with respect to the corresponding downhill rate. Then, during the first half of period *iii*, subunits 1 and 2 switched the energetic order and feature a relatively large mismatch in site energies of about 495 cm^{-1} (see Figure S7b). Now the uphill transfer runs from subunit 2 to 1, yet with a rate that is about an order of magnitude smaller than the downhill rate, resulting in an increase of the emission from subunit 2 and a simultaneous decrease of the emission from subunit 1. A kinetic scheme that yields qualitative agreement for the ratios between the fluorescence intensities from the subunits is presented in the Supporting Information (Figure S7).

Interestingly, the main changes of the emission properties, *i.e.*, here the site energy variations that influence the energy transfer pathways, affect predominantly the emission channel that is associated with one of the outer subunits (1 and/or 3). As these are more exposed to the polystyrene host than the central subunit, it is likely that these changes are induced by the matrix. Thermal fluctuations of the polymer chains around the trimer can give rise to conformational dynamics of the phenoxy-groups at the bay positions as well as at the butyl-chain at the imide group of PBI, and can alter the spectral properties of this subunit.[43,46,47]

Eventually, the energy transfer between subunits can be terminated by photobleaching of one of the components, which may result in the recovery of the signal from other neutral (nonbleached) subunits. In the examples shown here, this can be observed in Figure 4b during period *iii*, where the signal in the s-channel (associated with subunit 2) increases after photobleaching of subunit 1, and in Figure 5b during period *ii*, where the signal in the p-channel (associated with subunit 2) increases after photobleaching of subunits 1 and 3. As mentioned before, these observations are consistent with previous reports that the formation of a photoproduct does not necessarily quench the emission from an adjacent neutral subunit by energy transfer to the photoproduct.[32,33,45]

As a final remark, we note that our recent blinking studies of PBI dimers in a polymer host matrix revealed three different types of blinking, namely type 1, type 2 and type 3, which were categorized according to the chronological order of the variations of the signal levels in intensity trajectories.[41,43] Such different types of blinking reflect differences in the energy transfer rate between the neutral PBI and the reversibly formed radical anion, and we were able to associate the appearance of blinking types 1 to 3 with a decreasing free cavity volume of the host matrix around the dimer molecules. For the trimer molecules, in contrast, the majority of the trajectories (*e.g.*, those in Figures 3–5) exhibited type 1 blinking, *i.e.*, random intensity jumps between signal and background level, even during periods where multiple emitters are present, see for example periods *i* and *ii* in Figures 3 and 4 and period *i* in Figure 5. Hence, the trimer molecules are mostly located in large free volumes of the polymer matrix, which is reasonable due to their size and their bulky side groups. Consequently, predominantly type 1 blinking is to be expected as observed in our data.

CONCLUSIONS

In summary, we show that when polarization-resolved fluorescence intensity and spectral data are used, the intensity trajectories of multichromophores can be properly interpreted. The examples shown reveal that a PBI-trimer molecule can be subjected to sequential photobleaching as well as to a complex interplay between those photophysical parameters that determine the energy transfer dynamics within the trimers, even if this is not reflected in the total intensity trajectory. Further we observed emission from *all* photoactive subunits within the bin time of 300 ms in a trimer molecule rather than exclusively from the energetically lowest lying chromophoric site. We find that thermally activated uphill excitation energy transport processes repopulate the higher energy subunits.

METHODS

Bulk steady-state absorption and emission spectra of PBI monomers and trimers were measured in toluene (Sigma-Aldrich, 99.7%) using commercial spectrometers (absorption, Perkin-Elmer Lamda-750; emission, Varian Cary Eclipse). The emission spectra were excited at 532 nm.

Single-molecule samples were prepared from a solution of PBI trimers ($\sim 10^{-10}$ M) in toluene containing 5 mg/mL polystyrene. Thirty microliters of this solution was spin-coated on a freshly cleaned glass coverslip at 2500 rpm for 60 s. Individual trimers were excited with the output from a continuous-wave laser (Monopower 532-100-SM, Alphalas GmbH, Germany) operating at 532 nm *via* a home-built confocal microscope with an infinity-corrected oil-immersion objective (PlanApo, 60×, NA = 1.45, Olympus). To avoid preferential excitation of particular subunits of the trimers, the excitation was converted to circularly polarized light by a quarter-wave plate (Thorlabs GmbH). The excitation intensity was adjusted to 5 kW/cm^2 in the focal plane. The fluorescence emission from a single trimer was collected by the same objective, and passed through a dichroic beam splitter and a dielectric filter (z532RDC, 545 LP, AHF Analysentechnik AG) to suppress scattered excitation light.

The signal from the sample was directed through a Wollaston prism (angular deviation of 5°, Laser2000 GmbH) which resulted in two spatially separated signals with mutually orthogonal linear polarizations with respect to a laboratory frame. Both signals were focused onto the entrance slit of a spectrometer (SPEC 250IS, 150 grooves/mm, blaze wavelength 500 nm; Bruker Optics Inc., spectral resolution 1 nm at 600 nm) equipped with a back-illuminated electron-multiplying charge-coupled device camera (emCCD, iXon DV887-BI, Andor Technology). From each trimer, we typically registered successively 600 emission spectra with an exposure time of 300 ms. Each spectrum was fitted with a combination of two Gaussian functions, one for the purely electronic transition (0−0) and the second for the vibrational sideband, see Figure S3. This approach yields simultaneously the peak emission wavelength of the electronic 0−0 transition λ_{peak} as a function of time, and, by spectrally integrating the intensity of the individual spectra, the polarization-resolved fluorescence intensities, which will be referred to as I_p and I_s for the parallel (p) and the perpendicular (s) channel, respectively. We verified that the detection efficiency of our setup did not depend on the polarization of the fluorescence by recording polarization-resolved emission spectra of dye-loaded beads, Figure S4. Also we confirmed immobilization of molecules in a polymer matrix by performing polarization-resolved spectral measurements of individual monomers consisting of a PBI chromophore and a calix[4]arene bridge (compound **rc** from ref 26), Figure S5. We found a nearly constant ratio between the intensities in the p- and s-channels, I_p and I_s, indicating a spatially fixed transition dipole moment of the monomer. All experiments were carried out at room temperature.

Conflict of Interest: The authors declare no competing financial interest.

Acknowledgment. All authors gratefully acknowledge financial support from the state of Bavaria within the initiative 'Solar Technologies Go Hybrid'. A. Issac, R. Hildner and J. Köhler thank the Deutsche Forschungsgemeinschaft (GRK 1640) and the state of Bavaria (Elite Network of Bavaria: Macromolecular Science) for additional support.

Supporting Information Available: Synthesis of PBI trimer **3**, characterization by proton NMR spectroscopy, absorption and fluorescence spectra, polarization-resolved data of individual PBI trimer, dye loaded bead, and PBI monomers as well as kinetic scheme for down- and uphill energy transfer between two nonresonant chromophores. This material is available free of charge *via* the Internet at http://pubs.acs.org.

REFERENCES AND NOTES

1. Gross, M.; Müller, D. C.; Nothofer, H.-G.; Scherf, U.; Neher, D.; Bräuchle, C.; Meerholz, K. Improving the Performance of Doped π-Conjugated Polymers for Use in Organic Light-Emitting Diodes. *Nature* **2000**, *405*, 661–665.
2. Brabec, C. J.; Sariciftci, N. S.; Hummelen, J. C. Plastic Solar Cells. *Adv. Funct. Mater.* **2001**, *11*, 15–26.
3. Hüttner, S.; Sommer, M.; Thelakkat, M. n-Type Organic Field Effect Transistors from Perylene Bisimide Block Copolymers and Homopolymers. *Appl. Phys. Lett.* **2008**, *92*, 093302−1–3.
4. Peet, J.; Heeger, A. J.; Bazan, G. C. "Plastic" Solar Cells: Self-Assembly of Bulk Heterojunction Nanomaterials by Spontaneous Phase Separation. *Acc. Chem. Res.* **2009**, *42*, 1700–1708.
5. Brédas, J.-L.; Norton, J. E.; Cornil, J.; Coropceanu, V. Molecular Understanding of Organic Solar Cells: The Challenges. *Acc. Chem. Res.* **2009**, *42*, 1691–1699.
6. Wasielewski, M. R. Self-Assembly Strategies for Integrating Light Harvesting and Charge Separation in Artificial Photosynthetic Systems. *Acc. Chem. Res.* **2009**, *42*, 1910–1921.
7. Liu, H.; Xu, J.; Li, Y.; Li, Y. Aggregate Nanostructures of Organic Molecular Materials. *Acc. Chem. Res.* **2010**, *43*, 1496–1508.
8. Weil, T.; Vosch, T.; Hofkens, J.; Peneva, K.; Müllen, K. The Rylene Colorant Family—Tailored Nanoemitters for Photonics Research and Applications. *Angew. Chem., Int. Ed.* **2010**, *49*, 9068–9093.
9. Brovelli, S.; Meinardi, F.; Winroth, G.; Fenwick, O.; Sforazzini, G.; Frampton, M. J.; Zalewski, L.; Levitt, J. A.; Marinello, F.; Schiavuta, P.; *et al.* White Electroluminescence by Supramolecular Control of Energy Transfer in Blends of Organic-Soluble Encapsulated Polyfluorenes. *Adv. Funct. Mater.* **2010**, *20*, 272–280.
10. Basham, J. I.; Mor, G. K.; Grimes, C. A. Förster Resonance Energy Transfer in Dye-Sensitized Solar Cells. *ACS Nano* **2010**, *4*, 1253–1258.
11. Coffey, D. C.; Ferguson, A. J.; Kopidakis, N. Rumbles, G. Photovoltaic Charge Generation in Organic Semiconductors Based on Long-Range Energy Transfer. *ACS Nano* **2010**, *4*, 5437–5445.
12. Zhan, X.; Facchetti, A.; Barlow, S.; Marks, T. J.; Ratner, M. A.; Wasielewski, M. R.; Marder, S. R. Rylene and Related Diimides for Organic Electronics. *Adv. Mater.* **2011**, *23*, 268–284.
13. Würthner, F.; Stolte, M. Naphthalene and Perylene Diimides for Organic Transistors. *Chem. Commun.* **2011**, *47*, 5109–5115.
14. Wang, C.; Dong, H.; Hu, W.; Liu, Y.; Zhu, D. Semiconducting π-Conjugated Systems in Field-Effect Transistors: A Material Odyssey of Organic Electronics. *Chem. Rev.* **2011**, *112*, 2208–2267.
15. Würthner, F.; Kaiser, T. E.; Saha-Möller, C. R. J-Aggregates: From Serendipitous Discovery to Supramolecular Engineering of Functional Dye Materials. *Angew. Chem., Int. Ed.* **2011**, *50*, 3376–3410.
16. Sengupta, S.; Würthner, F. Chlorophyll J-Aggregates: From Bioinspired Dye Stacks to Nanotubes, Liquid Crystals, and Biosupramolecular Electronics. *Acc. Chem. Res.* **2013**, *46*, 2498–2512.
17. Didraga, C.; Klugkist, J. A.; Knoester, J. Optical Properties of Helical Cylindrical Molecular Aggregates: The Homogeneous Limit. *J. Phys. Chem. B* **2002**, *106*, 11474–11486.
18. Bredas, J. L.; Beljonne, D.; Coropceanu, V.; Cornil, J. Charge-Transfer and Energy-Transfer Processes in π-Conjugated Oligomers and Polymers: A Molecular Picture. *Chem. Rev.* **2004**, *104*, 4971–5003.
19. Laquai, F.; Park, Y.-S.; Kim, J.-J.; Basché, T. Excitation Energy Transfer in Organic Materials: From Fundamentals to Optoelectronic Devices. *Macromol. Rapid Commun.* **2009**, *30*, 1203–1231.
20. Beljonne, D.; Curutchet, C.; Scholes, G. D.; Silbey, R. J. Beyond Förster Resonance Energy Transfer in Biological and Nanoscale Systems. *J. Phys. Chem. B* **2009**, *113*, 6583–6599.
21. Scholes, G. D. Quantum-Coherent Electronic Energy Transfer: Did Nature Think of It First? *J Phys. Chem. Lett.* **2010**, *1*, 2–8.
22. Noriega, R.; Rivnay, J.; Vandewal, K.; Koch, F. P. V.; Stingelin, N.; Smith, P.; Toney, M. F.; Salleo, A. A General Relationship between Disorder, Aggregation and Charge Transport in Conjugated Polymers. *Nat. Mater.* **2013**, *12*, 1038–1044.
23. Vosch, T.; Fron, E.; Hotta, J.; Deres, A.; Uji-i, H.; Idrissi, A.; Yang, J.; Kim, D.; Puhl, L.; Haeuseler, A.; *et al.* Synthesis, Ensemble, and Single Molecule Characterization of a Diphenyl-Acetylene Linked Perylenediimide Trimer. *J. Phys. Chem. C* **2009**, *113*, 11773–11782.
24. Diehl, F. P.; Roos, C.; Duymaz, A.; Lunkenheimer, B.; Köhn, A.; Basché, T. Emergence of Coherence through Variation of Intermolecular Distances in a Series of Molecular Dimers. *J. Phys. Chem. Lett.* **2014**, *5*, 262–269.
25. Hippius, C.; Schlosser, F.; Vysotsky, M. O.; Böhmer, V.; Würthner, F. Energy Transfer in Calixarene-Based Cofacial-Positioned Perylene Bisimide Arrays. *J. Am. Chem. Soc.* **2006**, *128*, 3870–3871.
26. Hippius, C.; van Stokkum, I. H. M.; Gsänger, M.; Groeneveld, M. M.; Williams, R. M.; Würthner, F. Sequential FRET Processes in Calix[4]arene-Linked Orange-Red-Green

Perylene Bisimide Dye Zigzag Arrays. *J. Phys. Chem. C* **2008**, *112*, 2476–2486.
27. Bahng, H. W.; Yoon, M.-C.; Lee, J.-E.; Murase, Y.; Yoneda, T.; Shinokubo, H.; Osuka, A.; Kim, D. Ensemble and Single-Molecule Spectroscopic Study on Excitation Energy Transfer Processes in 1,3-Phenylene-Linked Perylenebisimide Oligomers. *J. Phys. Chem. B* **2011**, *116*, 1244–1255.
28. Schlosser, F.; Sung, J.; Kim, P.; Kim, D.; Würthner, F. Excitation Energy Migration in Covalently Linked Perylene Bisimide Macrocycles. *Chem. Sci.* **2012**, *3*, 2778–2785.
29. Sautter, A.; Kaletas, B. K.; Schmid, D. G.; Dobrawa, R.; Zimine, M.; Jung, G.; van Stokkum, I. H. M.; de Cola, L.; Williams, R. M.; Würthner, F. Ultrafast Energy-Electron Transfer Cascade in a Multichromophoric Light-Harvesting Molecular Square. *J. Am. Chem. Soc.* **2005**, *127*, 6719–6729.
30. Weil, T.; Wiesler, U. M.; Herrmann, A.; Bauer, R.; Hofkens, J.; de Schryver, F. C.; Müllen, K. Polyphenylene Dendrimers with Different Fluorescent Chromophores Asymmetrically Distributed at the Periphery. *J. Am. Chem. Soc.* **2001**, *123*, 8101–8108.
31. Flors, C.; Oesterling, I.; Schnitzler, T.; Fron, E.; Schweitzer, G.; Sliwa, M.; Herrmann, A.; van der Auweraer, M.; de Schryver, F. C.; Müllen, K.; *et al.* Energy and Electron Transfer in Ethynylene Bridged Perylene Diimide Multichromophores. *J. Phys. Chem. C* **2007**, *111*, 4861–4870.
32. Hofkens, J.; Maus, M.; Gensch, T.; Vosch, T.; Cotlet, M.; Köhn, F.; Herrmann, A.; Müllen, K.; de Schryver, F. C. Probing Photophysical Processes in Individual Multichromophoric Dendrimers by Single Molecule Spectroscopy. *J. Am. Chem. Soc.* **2000**, *122*, 9278–9288.
33. Gronheid, R.; Hofkens, J.; Köhn, F.; Weil, T.; Reuther, E.; Müllen, K.; de Schryver, F. C. Intramolecular Förster Energy Transfer in a Dendritic System at the Single Molecule Level. *J. Am. Chem. Soc.* **2002**, *124*, 2418–2419.
34. Lippitz, M.; Hübner, C. G.; Christ, T.; Eichner, H.; Bordat, P.; Herrmann, A.; Müllen, K.; Basché, T. Coherent Electronic Coupling *versus* Localization in Individual Molecular Dimers. *Phys. Rev. Lett.* **2004**, *92*, 103001.
35. Hernando, J.; Hoogenboom, J. P.; van Dijk, E. M. H. P.; Garcia-Lopez, J. J.; Crego-Calama, M.; Reinhoudt, D. N.; van Hulst, N. F.; Garcia-Parajo, M. F. Single Molecule Photobleaching Probes the Exciton Wave Function in a Multichromophoric System. *Phys. Rev. Lett.* **2004**, *93*, 236404.
36. Lang, E.; Sorokin, A.; Drechsler, M.; Malyukin, Y. V.; Köhler, J. Optical Spectroscopy on Individual Amphi-Pic J-Aggregates. *Nano Lett.* **2005**, *5*, 2635–2640.
37. de Schryver, F. C.; Vosch, T.; Cotlet, M.; Van der Auweraer, M.; Müllen, K.; Hofkens, J. Energy Dissipation in Multichromophoric Single Dendrimers. *Acc. Chem. Res.* **2005**, *38*, 514–522.
38. Métivier, R.; Nolde, F.; Müllen, K.; Basché, T. Electronic Excitation Energy Transfer between Two Single Molecules Embedded in a Polymer Host. *Phys. Rev. Lett.* **2007**, *98*, 047802.
39. Melnikov, S. M.; Yeow, E. K. L.; Uji-i, H.; Cotlet, M.; Müllen, K.; de Schryver, F. C.; Enderlein, J.; Hofkens, J. Origin of Simultaneous Donor–Acceptor Emission in Single Molecules of Peryleneimide–Terrylenediimide Labeled Polyphenylene Dendrimers. *J. Phys. Chem. B* **2007**, *111*, 708–719.
40. Park, M.; Yoon, M. C.; Yoon, Z. S.; Hori, T.; Peng, X. B.; Aratani, N.; Hotta, J. I.; Uji-I, H.; Sliwa, M.; Hofkens, J.; *et al.* Single-Molecule Spectroscopic Investigation of Energy Migration Processes in Cyclic Porphyrin Arrays. *J. Am. Chem. Soc.* **2007**, *129*, 3539–3544.
41. Ernst, D.; Hildner, R.; Hippius, C.; Würthner, F.; Köhler, J. Photoblinking Dynamics in Single Calix[4]arene-Linked Perylene Bisimide Dimers. *Chem. Phys. Lett.* **2009**, *482*, 93–98.
42. Yoo, H.; Furumaki, S.; Yang, J.; Lee, J.-E.; Chung, H.; Oba, T.; Kobayashi, H.; Rybtchinski, B.; Wilson, T. M.; Wasielewski, M. R.; *et al.* Excitonic Coupling in Linear and Trefoil Trimer Perylenediimide Molecules Probed by Single-Molecule Spectroscopy. *J. Phys. Chem. B* **2012**, *116*, 12878–12886.
43. Issac, A.; Hildner, R.; Ernst, D.; Hippius, C.; Würthner, F.; Köhler, J. Single Molecule Studies of Calix[4]arene-Linked Perylene Bisimide Dimers: Relationship Between Blinking, Lifetime and/or Spectral Fluctuations. *Phys. Chem. Chem. Phys.* **2012**, *14*, 10789–10798.
44. Lee, J.-E.; Stepanenko, V.; Yang, J.; Yoo, H.; Schlosser, F.; Bellinger, D.; Engels, B.; Scheblykin, I. G.; Würthner, F.; Kim, D. Structure Property Relationship of Perylene Bisimide Macrocycles Probed by Atomic Force Microscopy and Single-Molecule Fluorescence Spectroscopy. *ACS Nano* **2013**, *7*, 5064–5076.
45. Vosch, T.; Cotlet, M.; Hofkens, J.; van der Biest, K.; Lor, M.; Weston, K.; Tinnefeld, P.; Sauer, M.; Latterini, L.; Müllen, K.; *et al.* Probing Förster Type Energy Pathways in a First Generation Rigid Dendrimer Bearing Two Perylene Imide Chromophores. *J. Phys. Chem. A* **2003**, *107*, 6920–6931.
46. Hofkens, J.; Vosch, T.; Maus, M.; Köhn, F.; Cotlet, M.; Weil, T.; Herrmann, A.; Müllen, K.; de Schryver, F. C. Conformational Rearrangements in and Twisting of a Single Molecule. *Chem. Phys. Lett.* **2001**, *333*, 255–263.
47. Krause, S.; Aramendia, P. F.; Täuber, D.; von Borczyskowski, C. Freezing Single Molecule Dynamics on Interfaces and in Polymers. *Phys. Chem. Chem. Phys.* **2011**, *13*, 1754–1761.
48. Nirmal, M.; Dabbousi, B. O.; Bawendi, M. G.; Macklin, J. J.; Trautman, J. K.; Harris, T. D.; Brus, L. E. Fluorescence Intermittency in Single Cadmium Selenide Nanocrystals. *Nature* **1996**, *383*, 802–804.
49. Bopp, M. A.; Jia, Y.; Li, L.; Cogdell, R. J.; Hochstrasser, R. M. Fluorescence and Photobleaching Dynamics of Single Light-Harvesting Complexes. *Proc. Natl. Acad. Sci. U.S.A.* **1997**, *94*, 10630–10635.
50. Dickson, R. M.; Cubitt, A. B.; Tsien, R. Y.; Moerner, W. E. On/off Blinking and Switching Behaviour of Single Molecules of Green Fluorescent Protein. *Nature* **1997**, *388*, 355–358.
51. Cichos, F.; von Borczyskowski, C.; Orrit, M. Power-Law Intermittency of Single Emitters. *Curr. Opin. Colloid Interface Sci.* **2007**, *12*, 272–284.
52. Hoogenboom, J. P.; van Dijk, E.; Hernando, J.; van Hulst, N. F.; Garcia-Parajo, M. F. Power-Law-Distributed Dark States Are the Main Pathway for Photobleaching of Single Organic Molecules. *Phys. Rev. Lett.* **2005**, *95*, 097401.
53. Yeow, E. K. L.; Melnikov, S. M.; Bell, T. D. M.; De Schryver, F. C.; Hofkens, J. Characterizing the Fluorescence Intermittency and Photobleaching Kinetics of Dye Molecules Immobilized on a Glass Surface. *J. Phys. Chem. A* **2006**, *110*, 1726–1734.
54. Haase, M.; Hübner, C. G.; Nolde, F.; Müllen, K.; Basché, T. Photoblinking and Photobleaching of Rylene Diimide Dyes. *Phys. Chem. Chem. Phys.* **2011**, *13*, 1776–1785.
55. Hübner, C. G.; Zumofen, G.; Renn, A.; Herrmann, A.; Müllen, K.; Basché, T. Photon Antibunching and Collective Effects in the Fluorescence of Single Bichromophoric Molecules. *Phys. Rev. Lett.* **2003**, *91*, 093903.
56. Schroeyers, W.; Vallee, R.; Patra, D.; Hofkens, J.; Habuchi, S.; Vosch, T.; Cotlet, M.; Müllen, K.; Enderlein, J.; de Schryver, F. C. Fluorescence Lifetimes and Emission Patterns Probe the 3d Orientation of the Emitting Chromophore in a Multichromophoric System. *J. Am. Chem. Soc.* **2004**, *126*, 14310–14311.